PAPER

Check for updates

CuS@Cu-CD composites as efficient heterogeneous Fenton-like catalysts for the photodegradation of tetracycline

Yong Cheng, [iD] * Lin Deng, Dan Wang, Xiuxiu Wang, Changchun Ji and Ying-Hua Zhou

In this work, CuS@Cu-CD composites were synthesized and employed as Fenton-like catalysts. CuS significantly enhanced the photodegradation activity of tetracycline (TC) when decorated with Cu-doped-carbon dots (Cu-CDs). The influence of initial pH, dosage of catalyst, and H_2O_2 concentration on the catalyst performance was investigated. Radical trapping experiments proved that $\cdot O_2^-$ and h^+ played critical roles and $\cdot OH$ played a moderate role in the degradation of TC. Mechanism analyses demonstrated that Cu^{2+}/Cu^+ redox circulation could be accelerated by the introduction of Cu into carbon dots, which further facilitated H_2O_2 consumption and resulted in higher TC degradation efficiency.

Environmental significance

Tetracycline (TC) is widely used as a broad-spectrum antibiotic for treating a wide range of diseases. However, the continuous abuse and overuse of TC results in environmental pollution. Photocatalysis is one of the environmentally friendly and sustainable strategies to eliminate TC pollution. Here, we have successfully developed a novel CuS@Cu-CD composite to act as an efficient heterogeneous Fenton-like catalyst for the photocatalytic degradation of tetracycline in solution with the assistance of H_2O_2. It provides important insights into photocatalytic devices, promoting the further development of unconventional Fenton-like catalysts in the catalytic field.

Introduction

Organic chemicals, which may be found as pollutants in wastewater effluents from industrial or domestic sources, must be removed or destroyed before discharge into the environment. The Fenton process is considered to be the most powerful catalytic technology for oxidative degradation of organic contaminants.[1] However, the classical Fenton processes suffer from the problems of poor activity under neutral conditions and excessive consumption and waste of H_2O_2 due to the restriction of the electron cycle caused by the rate limiting pathway for the high-valence metal reduction by H_2O_2.[2] Recently, Fenton-like catalysts with electron-rich metal centers such as Cu, Ru, Mn, Co, and Ce have attracted considerable attention because they have the same effect as iron.[3] Copper with multiple valences (Cu^0, Cu^+, and Cu^{2+}) has shown to be a promising candidate to catalyze Fenton-like reactions by virtue of its favorable redox ability and higher electron transfer rate than Fe(II)/Fe(III) and better solubility of Cu^{2+} than Fe^{3+} in water, as well as reduced generation of metal solid wastes. A variety of copper-based

composites have been reported and applied to degrade organic pollutants.[4–10] For example, $Cu_2O–Cu/C$ can degrade methyl orange, methyl blue, and rhodamine B in aqueous solutions in the presence of H_2O_2.[11] The Cu^+–graphitic carbon nitride complex exhibits an efficient Fenton-like activity for the removal of Rhodamine B from the aqueous solution.[12] The experimental results show that $CDs@CuO_x$ can trigger the Fenton reaction and increase the reaction velocity by nearly 35 times compared with CuO_x alone.[13] Even so, the design and synthesis of more efficient Cu-based Fenton-like catalysts are still actively pursued.

As is well known, electron transfer plays a key role in Fenton/Fenton-like chemistry. Utilizing electrons to enhance reaction efficiency is a strategy used to optimize the photocatalytic performance of Fenton-like catalysts.[14] Copper sulfide (CuS), a semiconductor material, can be excited upon light irradiation and produce photogenerated electrons and holes.[15] Carbon materials such as carbon dots with abundant electrons and strong electron transfer abilities are natural adjuvants for accelerating the high valence metal ion reduction process.[16] Furthermore, it has been found that the doping of metal promoted electron transfer and enhanced the performance of carbon dots in photo-oxidation reactions.[17] We assumed that the strategy of integrating copper-doped carbon dots (Cu-CDs) with CuS would endow the composites with the eminent

The Key Laboratory of Functional Molecular Solids, Ministry of Education, Anhui Laboratory of Molecule-Based Materials (State Key Laboratory Cultivation Base), College of Chemistry and Materials Science, Anhui Normal University, Wuhu, 241002, China. E-mail: chyong2008happy@163.com

© 2023 The Author(s). Published by the Royal Society of Chemistry

Environ. Sci.: Adv., 2023, **2**, 495–507 | **495**

properties of CDs and CuS. It is worth exploring in depth their photocatalytic activity.

Herein, we present CuS@Cu-CD composites in which Cu-CDs act as decorated accessories to heighten the photocatalytic activity of CuS. Related studies show that the composites are excellent catalysts to photodegrade tetracycline (TC) with the assistance of H_2O_2. The degradation mechanism and kinetics were also investigated. The enhanced photocatalytic performances were ascribed to the doped copper in CDs, which accelerated the electron transfer rate and CuS generated electron (e^-) and hole (h^+) carriers under the irradiation to form chemical active radicals superoxide radical ($\cdot O_2^-$) and hydroxyl radical ($\cdot OH$) to attack pollutants directly. These results provide important insights into photocatalytic devices, promoting the further development of unconventional Fenton-like catalysts in the catalytic field.

Experimental

Materials

Reagents and solvents employed were commercially available and used as received. $CuCl_2$, $Cu(Ac)_2$, folic acid, and DMF (AR grade) were purchased from Shanghai Lingfeng Chemical Reagent Co., Ltd., China. Thiourea, H_2O_2, $K_2S_2O_8$, disodium ethylenediaminetetraacetic acid (EDTA-2Na), p-benzoquinone (BQ), and $tert$-butanol (TB) were purchased from the Tianjin Chemicals Company and used as received. Tetracycline hydrochloride (TC) was purchased from Aladdin Chemical Reagent Co., Ltd. Water was deionized and bi-distilled.

Characterization

Fourier transform infrared spectroscopy (FT-IR) was recorded on a Nicolet iZ10 FT-IR spectrophotometer (Thermo Electron Co., USA). X-ray diffraction (XRD) patterns were recorded on a German Brooke XRD-D8 Advance D8 with Cu Kα radiation ($\lambda = 0.15406$ nm, voltage 40 kV, current 40 mA). Ultraviolet-visible (UV-vis) spectra experiments were performed on Hitachi UV-vis 3010 spectrophotometer (Hitachi Ltd. Tokyo, Japan). The morphology and microstructure of the samples were characterized by scanning electron microscopy (SEM, Hitachi Ltd. Tokyo, Japan) and field emission scanning electron microscopy (FESEM, Hitachi S-4800, Hitachi Ltd. Tokyo, Japan). X-ray photoelectron spectroscopy (XPS, Thermo Scientific, EscaLab 250Xi spectrometer, America) with a monochromatic Al Kα X-ray source was used to analyze elements ($h\nu = 1486.6$ eV, power 150 W, beam spot 650 μm, voltage 14.8 kV, current 1.6 A, and testing software is avantage). Photoluminescence spectroscopy (PL) was carried out using a Hitachi F-4500 fluorescence spectrophotometer (Hitachi Ltd. Tokyo, Japan). UV-vis diffuse reflectance spectroscopy (DRS) was performed in absorption mode at 200–800 nm by a Shimadzu UV-2450 spectrometer (Shimadzu Ltd. Japan). Electrochemical tests were carried out on a CHI760E electrochemical analyzer (CHIIns., Chenhua Ltd., Shanghai, China) in a conventional three-electrode configuration with a Pt foil as the counter electrode and Ag/AgCl (saturated KCl) as the reference electrode.

Synthesis of Cu-CDs

Folic acid (0.1 g) and DMF (10 mL) were mixed with $CuCl_2$ (0.05 g). The solution was stirred and then transferred to a 25 mL Teflon steel autoclave and heated at 190 °C for 12 h. The solution of Cu-CDs was obtained by dialysis against deionized water through a dialysis bag (MWCO: 1000 Da). It was evaporated to dryness for further use. A control sample without metal doping (bare CDs) was prepared under conditions similar to that of Cu-CDs.

Synthesis of CuS@Cu-CDs

CuS was prepared based on a previous report with some modifications.[18] $Cu(Ac)_2$ (0.3993 g, 3.5 mmol) and thiourea (0.1522 g, 3.5 mmol) were dissolved in ultrapure water (10 mL) and stirred continuously to form a microemulsion. Then, the mixture was transferred to a Teflon-lined autoclave (15 mL) and heated at 160 °C for 10 h. Afterwards, the mixture was cooled to room temperature naturally. The obtained black powder product was washed several times with ultrapure water and ethanol, respectively, and then dried in a vacuum oven and stored for later use.

100 mg CuS was added to the suspension of Cu-CDs (30 mg, 100 mL H_2O), then subjected to ultrasound for 20 min to obtain the final product CuS@Cu-CDs. CuS@CD composites were obtained with the same procedures for comparison.

Photocatalytic degradation of tetracycline

The photocatalytic activity of CuS@Cu-CD composites was determined by the photodegradation of TC. The mixture was irradiated by a 500 W xenon lamp for photodegradation under stirring. In a typical process, 10 mg of photocatalyst CuS@Cu-CDs was added to 100 mL of the TC solution and stirred for 60 min in the dark to attain the adsorption/desorption equilibration. For the photocatalytic process, 3 mL mixture was extracted and centrifuged to obtain clear liquor for the next residual TC detection using the spectrophotometer at a maximum absorption wavelength of 371 nm. Photocatalytic efficiency was calculated by the following formula:

$$\text{Photocatalytic efficiency} = \frac{(C_0 - C)}{C_0} \times 100$$

where C_0 and C represent concentrations of TC before and after irradiation, respectively.

Additives that could scavenge different active radicals were utilized in comparative trials to illuminate the degradation process of TC. $AgNO_3$ (1 mmol L^{-1}), disodium ethylenediaminetetraacetic acid (EDTA-2Na, 1 mmol L^{-1}), p-benzoquinone (BQ, 1 m mol L^{-1}), and $tert$-butanol (TBA, t-BuOH, 1 mmol L^{-1}) were introduced into the Fenton-like reaction system to capture electrons (e^-), holes (h^+), superoxide anion free radicals ($\cdot O_2^-$), and hydroxyl free radicals ($\cdot OH$). These tests were performed following the photocatalytic degradation process mentioned above.

Fenton-like reaction

Degradation experiments were carried out at room temperature (approximately 25 °C). The solution pH was adjusted by HCl

(0.1 mol L^{-1}) or NaOH (0.1 mol L^{-1}). In each experiment, 100 mg catalyst was added to the TC aqueous solution (10 mg L^{-1}, 100 mL), followed by the addition of 1 mL of H$_2$O$_2$ (30%) into the solution to initiate the Fenton-like reaction. Before illumination, the suspensions were magnetically stirred in the dark for 30 min to ensure the establishment of an adsorption–desorption equilibrium between the catalyst and TC. The sampling analysis was conducted in 10 min intervals, and a 3 mL suspension was sampled and centrifuged to remove the catalyst particles. The TC degradation efficiency (η) was calculated by η (%) = $(1 - C_t/C_0) \times 100\%$, where C_0 and C_t are the TC concentrations at the initial time and time t, respectively.
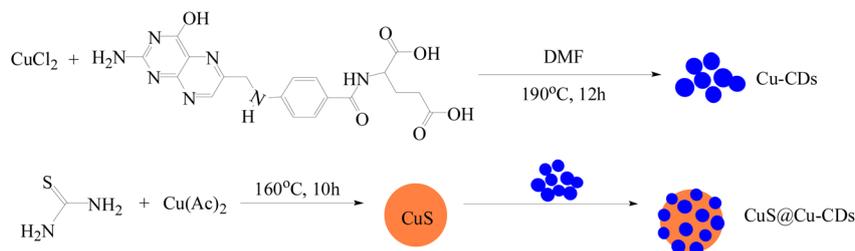
Results and discussion

Synthesis of CuS@Cu-CDs

Two-step procedures have been used to prepare CuS@Cu-CD composites, as shown in Scheme 1. Copper-doped carbon dots (Cu-CDs) were obtained by pyrolysis of the mixture of

CuCl$_2$ and folic acid in DMF, in which cupric ions can coordinate with the –COOH groups on the surface of carbon dots, forming a π-electron conjugated system *via* the C–O–Cu bond.[19] CuS was prepared by heating the mixture of Cu(Ac)$_2$ and thiourea. Then, it was added to the suspension of Cu-CDs and ultrasound to form CuS@Cu-CDs, in which CuS wrapped the Cu-CDs.

Characterization of CuS@Cu-CDs

Powder X-ray diffraction (PXRD) was used to evaluate the structure and phase composition of CuS@Cu-CDs and other related materials. On the 2θ scale, a broad diffraction peak was observed around $2\theta = 25°$, which is related to the graphitic (002) peak (Fig. 1a). For the pure CuS, the major diffraction peaks were found at $2\theta = 27.7°$, 29.3°, 31.8°, 32.9°, 47.7°, 47.9°, 52.7°, and 59.4°, which were well indexed to (101), (102), (103), (006), (007), (110), (108), and (116) crystal planes of covellite CuS (JCPDS no. 06-0464),[20] and revealing that adding CDs or Cu-CDs did not change the molding of CuS. The intense and sharp

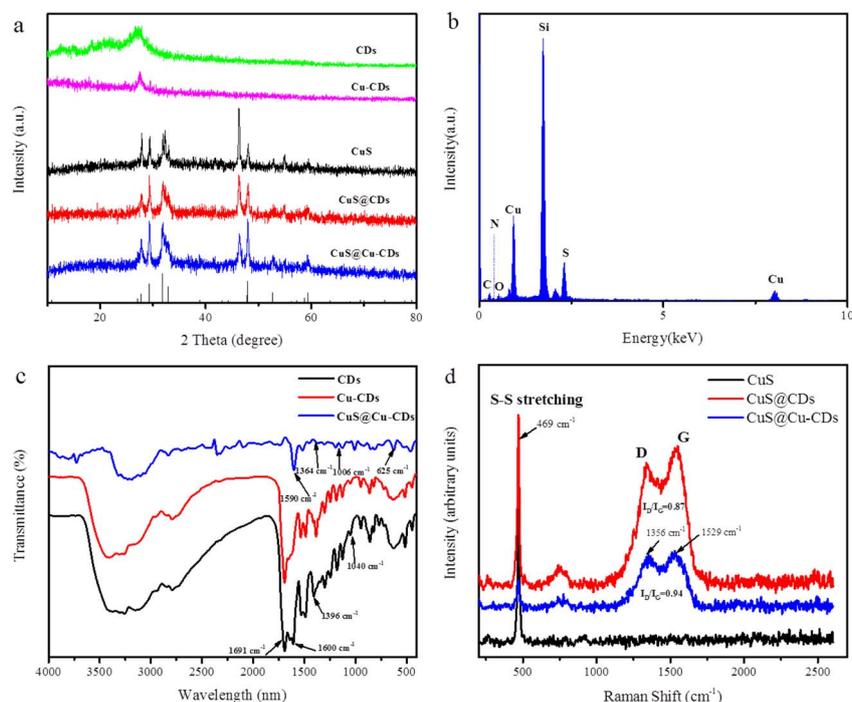
Scheme 1 Synthesis of CuS@Cu-CDs.

Fig. 1 (a) XRD (b) EDX (c) IR (d) Raman spectra of CuS@Cu-CDs.

© 2023 The Author(s). Published by the Royal Society of Chemistry

Environ. Sci.: Adv., 2023, **2**, 495–507 | **497**

diffraction peaks in the XRD patterns manifested high crystallinity of the CuS component. However, the XRD peaks of CDs and Cu-CDs were not observed in CuS@Cu-CDs due to the weak diffraction intensity and less content of CDs. Energy-dispersive X-ray spectroscopy (EDX) was performed on the as-prepared composites, which determined the elemental composition to comprise Cu (43.81), N (2.55), O (2.45), C (14.78), and S (11.24) wt% (Fig. 1b).

As shown in Fig. 1c, the black and red lines represent CDs and Cu-CDs, respectively, in the FT-IR spectra. The broad peaks centered at around 3100–3500 cm^{-1} were assigned to the stretching vibrations of O–H and –NH$_2$.[21–23] The typical peaks at 1600 cm^{-1} and 1691 cm^{-1} were associated with the stretching vibrations of C=N and C=O.[24] The peaks at 1396 cm^{-1} and 1040 cm^{-1} were ascribed to the vibration of C–O.[25] These typical peaks of CDs were also observed in CuS@Cu-CDs. Beyond that, the peak at 625 cm^{-1} was assigned to the stretching band of Cu–S.[26] These results indicated that CuS@Cu-CD composites were successfully synthesized.

The Raman spectra of CuS@Cu-CDs exhibit two bands at 1529 cm^{-1} and 1356 cm^{-1}, as shown in Fig. 1d. They were assigned to the D (sp^3-hybridized) and G (sp^2-hybridized) bands of the Cu-CDs. The D band was related to the vibrations of carbon atoms with dangling bonds in the termination plane of disordered graphite or glassy carbon.[27,28] The G band was associated with the vibration of sp^2-hybridized carbon atoms.[29] The intensity ratio of the disordered D band to the crystalline G band (I_D/I_G) was 0.87, indicating that it had a structure similar to graphite. It demonstrated that the intensity of the G band decreased with the addition of Cu into CDs (Fig. 1d). With Cu^{2+} doping into CDs, they chelated with carboxyl groups on the surface of CDs, which affected the in-plane stretching vibration of sp^2 hybridized C atoms of CDs. A sharp peak at 469 cm^{-1} is attributed to the S–S stretching vibration in CuS, which was consistent with the previous result.[30] There were no additional impurity peaks present for any copper substrate and unreacted precursor compound. It indicated that the CuS@Cu-CD composites were synthesized successfully.

SEM image illuminated that the morphologies of CuS and CuS@Cu-CDs were spherical in shape with a size of about 10–20 nm (Fig. 2a and b). The nanosphere was rough owing to the aggregation of CuS nanoparticles. The TEM image of Cu-CDs exhibited that the carbon dots had good monodispersity with a size < 5.0 nm (Fig. 2c). CuS@Cu-CDs sample showed that Cu-CDs deposited or inlaid on the CuS nanosphere as small dots (Fig. 2d). Fig. 3a–f are the elemental mapping diagrams of Cu, S, C, O, and N in CuS@Cu-CDs, respectively. It can be seen from the figures that these elements were evenly distributed on the hybrid material. These findings suggest that CuS is a good supporting matrix for Cu-CDs.

The chemical composition and valence states of CuS@Cu-CDs were characterized by XPS. As shown in Fig. 4a, the survey spectrum displayed that the main component elements of CuS@Cu-CDs were C, O, S, N, and Cu. The "shakeup" peak of the Cu^{2+} satellite is obviously observed at a binding energy of 943.1 eV. The peak at 933.3 eV corresponded to the oxidation of copper species (Cu^{2+}), whereas the peak located at 932.2 eV corresponds to the reduced copper species (Cu$^+$) according to previous reports,[31,32] and the ratio of Cu^{2+}/Cu$^+$ equals to 1.98 : 1 (Fig. 4b). These results signified that both Cu^{2+} and Cu$^+$ existed in CuS@Cu-CDs and the efficiency of the Fenton-like reaction might be regulated by the cycle of Cu^{2+}/Cu$^+$. XPS spectrum of S$_{2p}$
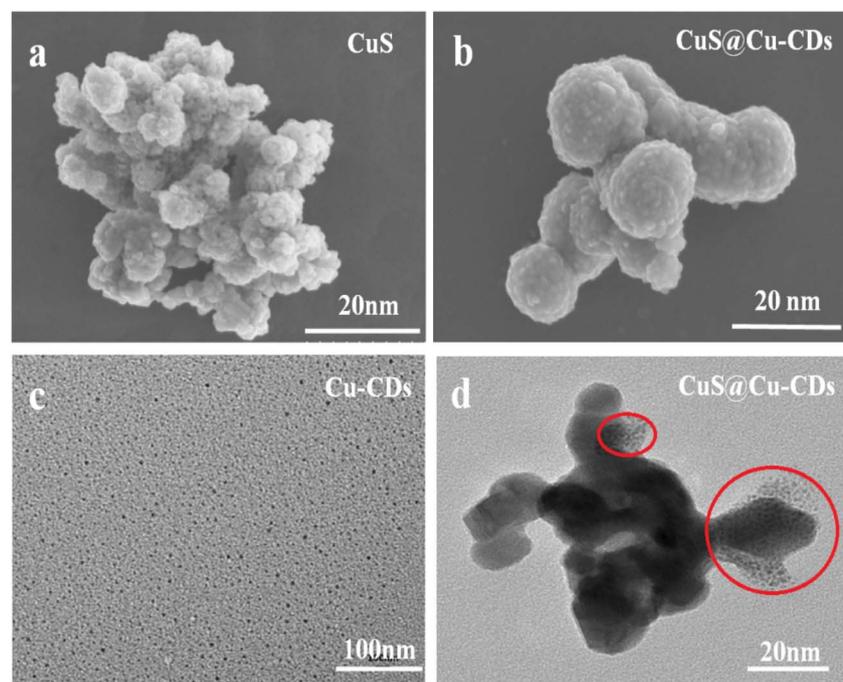

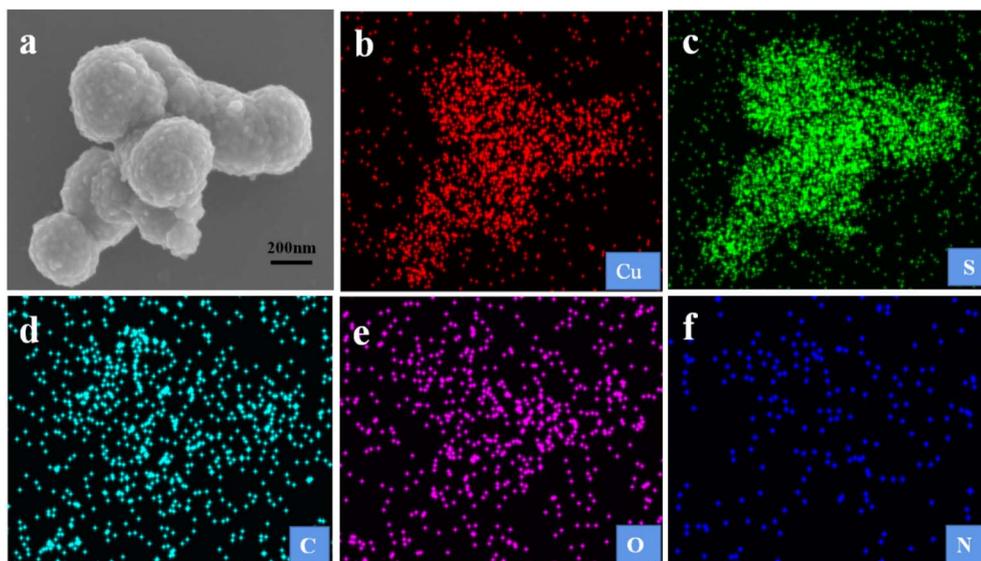Fig. 2 SEM of (a) CuS (b) CuS@Cu-CDs and TEM of (c) Cu-CDs (d) CuS@Cu-CDs.

Fig. 3 Mapping of (a) CuS@Cu-CDs (b) Cu (c) S (d) C (e) O (f) N.

was split into two peaks centered at 161.75 eV and 162.9 eV, which correspond to the binding energy of S $2p_{3/2}$ and S $2p_{1/2}$ states for S^{2-} in CuS (Fig. 4c).[33] C 1s spectrum was fitted into three separate peaks, which were located at 284.7 eV, 285.7 eV, and 288.2 eV, corresponding to C–C, C–O and C=O, respectively (Fig. 4d).[34] The peaks of O 1s are centered at 531.3 and 532.3 eV, which are aligned with the literature (Fig. 4e).[35] The high-resolution spectrum of N 1s revealed a dominant peak at 398.9 eV, which deconvoluted into two peaks at 398.7 eV and 400.1 eV and corresponded to N–C or N–H, respectively (Fig. 4f).[36] These results showed that the Cu-CDs were successfully loaded on CuS, fully consistent with that obtained from various characterizations.

The optical absorption properties of CuS@Cu-CDs, CuS, and Cu-CDs are exhibited in Fig. 5a. Cu-CDs and CuS@Cu-CDs displayed solar energy absorbance and their band edges approximately at 520 nm, while CuS clearly showed adsorption ability in the full spectrum region. The observation indicated that the absorption range of CuS@Cu-CDs was slightly wider than that of Cu-CDs. The band gap energies (E_g) of direct transition semiconductors can be calculated according to the plot of $(\alpha h\nu)2$ *versus* photon energy ($h\nu$).[37] As shown in Fig. 5b, the E_g of CuS@Cu-CDs is estimated to be 2.09 eV, which was wider than that of CuS (1.83 eV). It denoted that the Cu-CDs addition in CuS can promote their solar energy absorption.

The fluorescence spectra of the CDs and Cu-CDs exhibited emission peaks centered at around 450 nm (Fig. 6a and b). The absorbance intensity of Cu-CDs increased due to the introduction of Cu into CDs. It is well known that the radius of each arc is relevant to the charge-transfer resistance: the smaller the radius of the arc, the lower the corresponding impedance.[38] CuS@Cu-CDs showed the smallest charge-transfer resistance than CuS and CuS@CDs, coinciding with the conclusion of the EIS results (Fig. 6c). The transient photocurrent responses were employed to further explore the separation efficiency of photogenerated charge carriers.[39] In comparison with CuS and CuS@CDs, CuS@Cu-CDs exhibited the highest photocurrent density (Fig. 6d). It can generate considerably enhanced photocurrents with three visible-light irradiation on–off cycles.

Catalytic performance of CuS@Cu-CDs

Tetracycline has drawn widespread concern in society. It is widely used as a broad-spectrum antibiotic for treating a wide range of diseases. However, the continuous abuse and overuse of TC result in environmental pollution.[40–42] Photocatalysis is one of the environmentally friendly and sustainable strategies to eliminate TC pollution.

TC degradation by the as-prepared catalyst was carried out to investigate the reaction conditions. The experimental results are presented in Fig. 7a. Before the photocatalysis experiments, the suspension containing the catalyst and TC was magnetically stirred in the dark for 60 min to ensure an adsorption–desorption equilibrium without illumination.

The photolysis of TC can be neglected in the absence of a catalyst, which indicates that TC was very stable and hardly decomposed. About 5%, 10%, and 20% of TC were adsorbed on the surface of CuS, CuS@CDs, and CuS@Cu-CDs, respectively, in the part of the adsorption/desorption equilibrium experiment. Obviously, the adsorption ability of CuS@Cu-CDs is higher than that of CuS. TC degradation performance greatly improved (85%) under a Fenton-like system by CuS@Cu-CD composites. This acceleration is compactly related to the produced photoelectrons on the semiconductor CuS surface along with its intrinsic Cu^{2+}/Cu^+ circulation during catalysis reaction, which indicated that Cu-CDs introduction contributed to catalytic activity in the composites. Kinetics also show that significant degradation of TC occurred when CuS hybridized with Cu-CDs (Fig. 7b).

Catalyst dosage, which is strongly associated with the quantities of active sites, is a key parameter in a Fenton-like
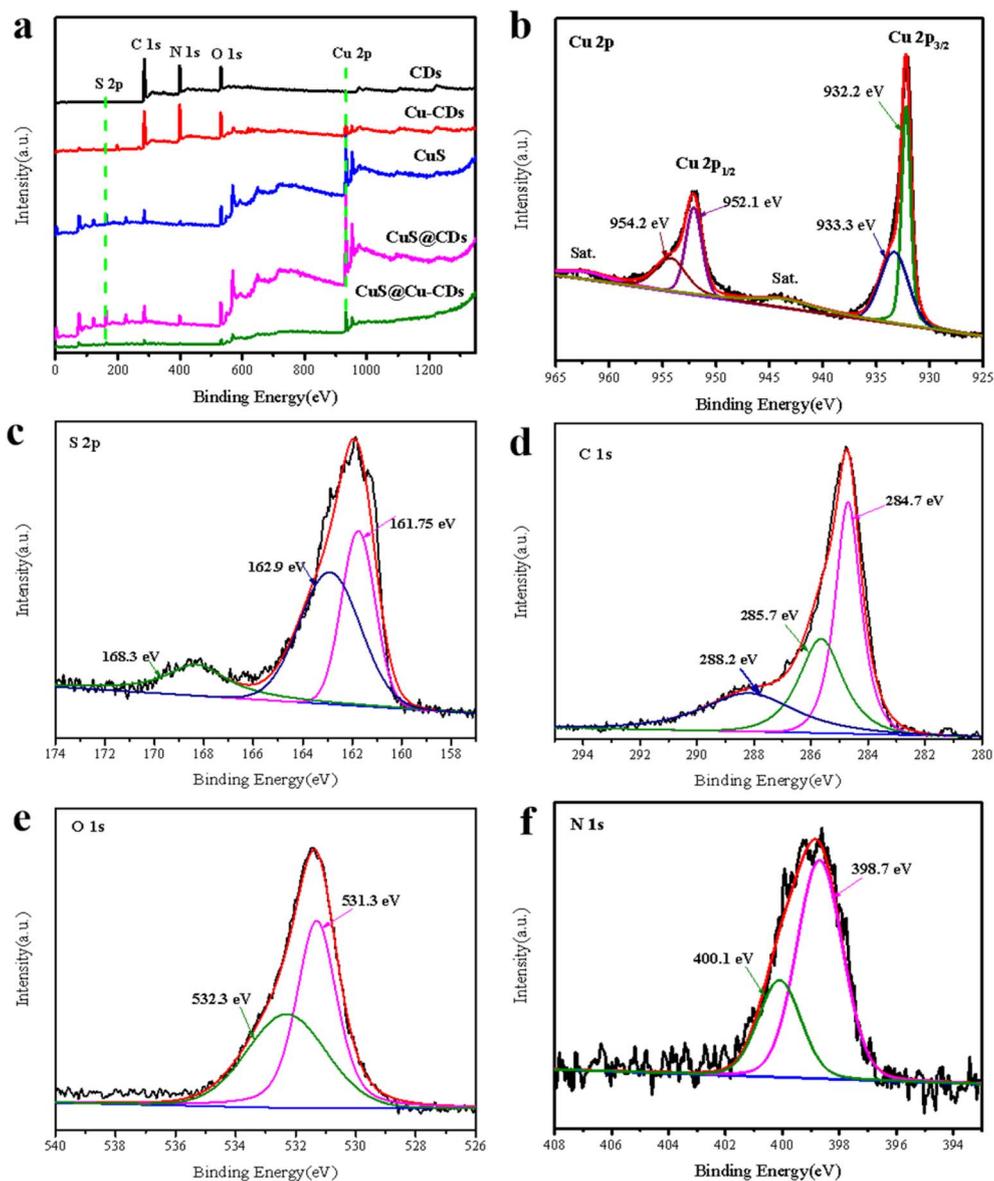
© 2023 The Author(s). Published by the Royal Society of Chemistry

Environ. Sci.: Adv., 2023, **2**, 495–507 | **499**

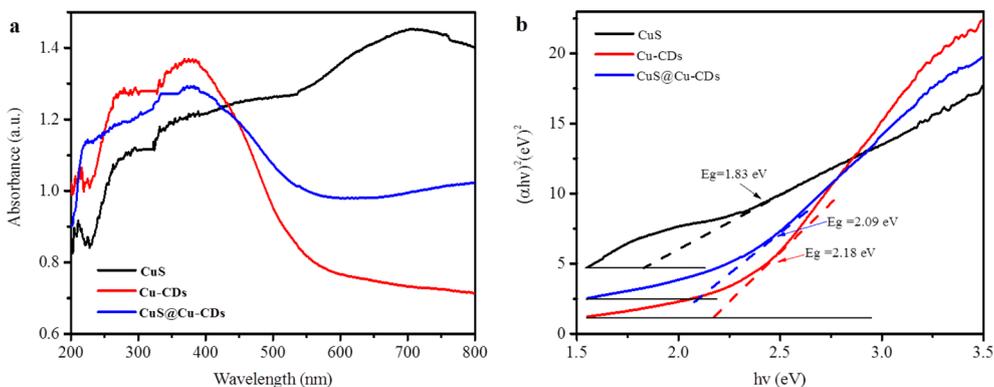**Fig. 4** XPS (a) survey spectrum (b) Cu 2p (c) S 2p (d) C 1s (e) O 1s (f) N 1s.

Fig. 5 (a) UV-vis DRS of prepared catalysts (b) plot of $(\alpha h\nu)^2$ *versus* $h\nu$ of CuS@Cu-CDs and its valence band spectra.
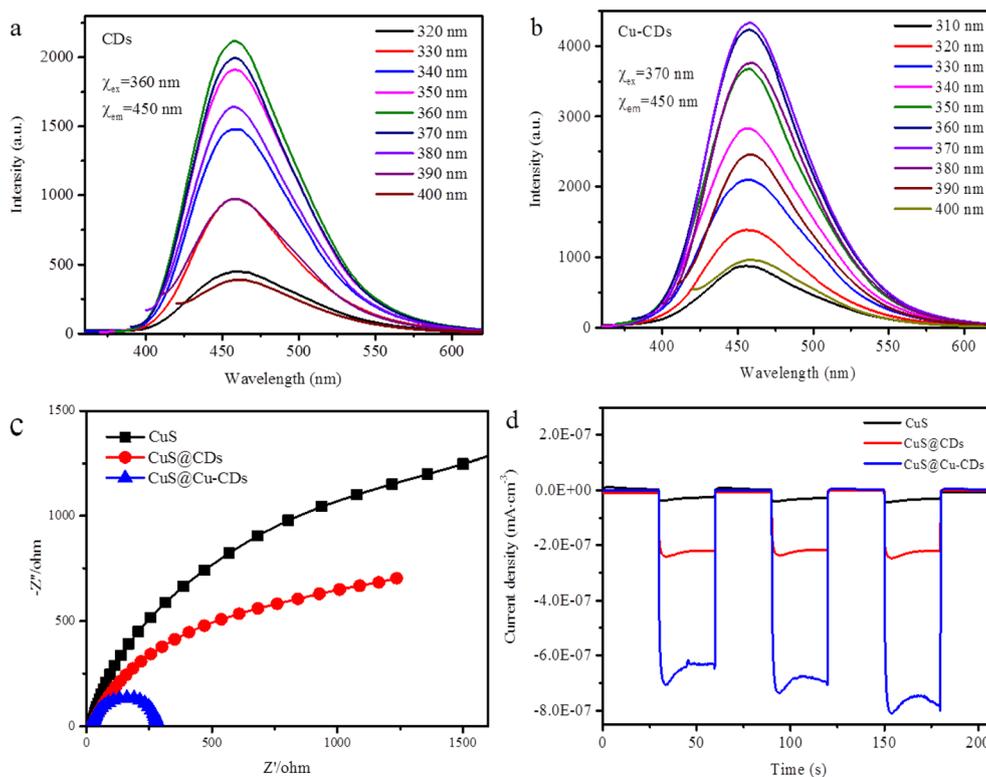
Paper

Fig. 6 Fluorescence emission of (a) CDs (b) Cu-CDs. (c) Electrochemical impedance spectrum and (d) transient photocurrent response of CuS@Cu-CDs.

degradation reaction.[43] Fig. 7c depicted the influence of catalyst dosage on TC catalytic degradation at pH 5.6. TC removal efficiency shows a significant increase from 70% to 80% in 30 min, with the catalyst dosage rising from 10 mg to 50 mg. Indeed, more catalyst means more active sites for H_2O_2 decomposition, hence facilitating organics degradation. However, an overdose of catalyst would lead to unsuitable radical consumption *via* the reactions (eqn (1) and (2)) as follows:[44]

$$Cu^+ + \cdot OH \rightarrow Cu^{2+} + OH^- \quad (1)$$

$$Cu^{2+} + \cdot O_2^- \rightarrow Cu^+ + O_2 \quad (2)$$
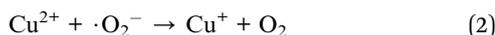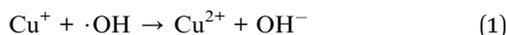
In the traditional Fenton system, the organic oxidation efficiencies are remarkably associated with the solution pH. Besides, tetracycline is sensitive to pH. Thus, the effect of initial pH on TC degradation in this Fenton-like system was investigated. As shown in Fig. 7d, the highest degradation efficiency of TC was achieved at pH = 5.6 in the initial 30 min, and the efficiencies decreased in the order of pH (5.6) > pH (3.2) > pH (7.2) > pH (9.3). Under acidic conditions, the reaction depicted in eqn (3) will easily occur. The reaction in eqn (4) would be inhibited and the generation rate of ·OH would be reduced. Therefore, the catalytic activity becomes weak under pH = 3.2, as shown in Fig. 7d. Furthermore, increased pH also leads to decreased ·OH oxidation potential. As for basic conditions around 9.3, the relatively lower degradation efficiency could be caused by the fact that hydroxyl radical has a redox potential of +2.8 V in acidic media and +1.5 V in basic media.[45]

$$4Cu^+ + 4H^+ + O_2 \rightarrow 4Cu^{2+} + 2H_2O \quad (3)$$

$$Cu^+ + H_2O_2 \rightarrow Cu^{2+} + \cdot OH + OH^- \quad (4)$$
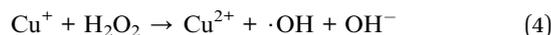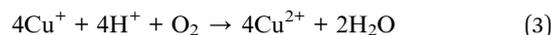
The effect of H_2O_2 concentration on TC oxidation process was also explored, and the results are presented in Fig. 7e. When H_2O_2 concentration increased from 5 mM to 7 mM, TC oxidative efficiency evidently enhanced (from 60% to 85%). This stated the fact that higher H_2O_2 concentration leads to sufficient $\cdot O_2^-$ for attacking the TC molecules. However, with H_2O_2 concentration continuously increasing to 10 mM, the degradation rate of TC declined to 70%. This is because the redundant H_2O_2 can be a scavenger of hydroxyl radicals (eqn (5)). Similar results were also reported in Fenton-like systems for antibiotic oxidative degradation.[43]

$$H_2O_2 + \cdot OH \rightarrow HO_2^\bullet + H_2O \quad (5)$$
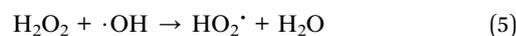
Various inorganic anions and other substances may coexist in wastewater and potentially affect the Fenton-like photocatalytic activity. Fig. 7f displays TC degradation curves in the presence of four typical anions (Cl^-, NO_3^-, SO_4^{2-}, and CO_3^{2-}) and natural water (river or tap water). NO_3^- and Cl^- displayed relatively weak impacts on the TC degradation procedure,[46] while SO_4^{2-} and CO_3^{2-} weakened TC degradation rates from 50.3% and 80.0%, respectively. SO_4^{2-} can be adsorbed onto the CuS surface to compete for active sites with TC molecules. CO_3^{2-} quenched ·OH with the formation of less-reactive radicals of $\cdot CO_3^{2-}$ *via* eqn (6).[47,48]

© 2023 The Author(s). Published by the Royal Society of Chemistry

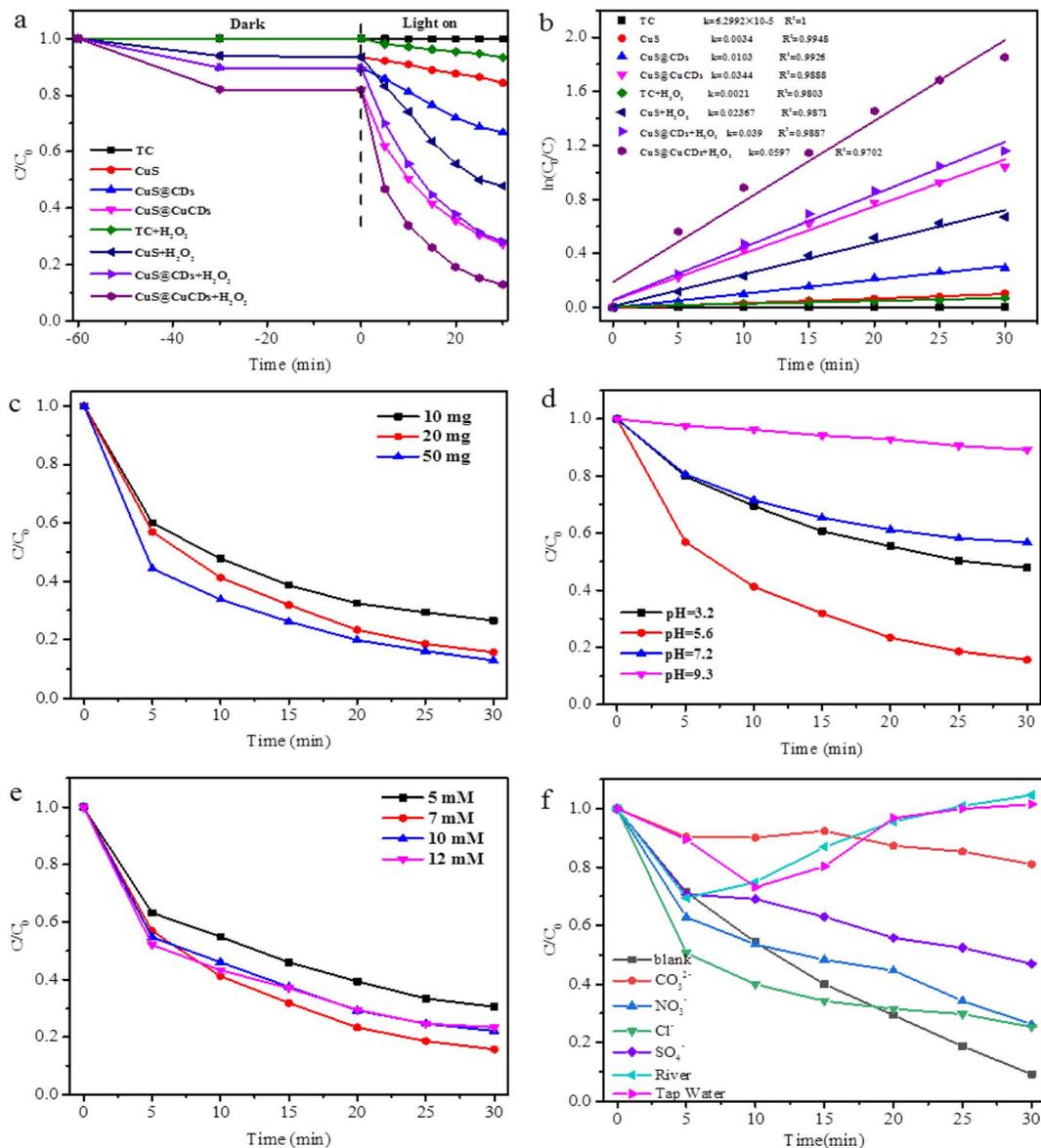*Environ. Sci.: Adv.*, 2023, **2**, 495–507 | **501**

Fig. 7 (a) TC degradation in various reaction systems (b) linear relationship of degradation kinetics over CuS@Cu-CDs and related materials (c) TC degradation with different catalyst dosages (d) with different initial pH (e) with different H_2O_2 concentrations (f) effect of different inorganic anions, natural water, and tap water on TC degradation by CuS@Cu-CDs ([anion concentration] = 20 mM; [catalyst dosage] = 20 mg; [H_2O_2] = 7 mM; [TC] = 20 mg L^{-1}; pH = 5.6).

$$CO_3^{2-} + \cdot OH \rightarrow \cdot CO_3^{2-} + OH^- \tag{6}$$
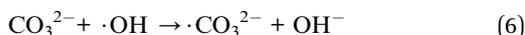
The catalytic activities were further analyzed using natural water (river water obtained from Huajing river in the campus of Anhui Normal University) and tap water (from Water Company, Wuhu) as the base. The TC removal efficiency was interfered with in an actual water body compared to ideal ultrapure water, and this might be closely associated with their water qualities of anions and pH.

Table 1 lists a comparison of removal efficiencies of tetracycline in the present work with some reported Fenton-like catalysts.[43,49–51] As displayed, our designed catalyst exhibits relatively higher catalytic activity than those reported in the literature for the photodegradation of TC in the water.

Active radical identification

In order to ascertain the reactive species that directly participate in the CuS@Cu-CDs photocatalytic system, active species trapping experiments were performed (Fig. 8a). In this research, *tert*-butylalcohol (TBA), *p*-benzoquinone (BQ), ethyl-enediaminetetraacetic acid disodium (EDTA-2Na), and AgNO$_3$ were employed as scavengers of hydroxyl radicals ($\cdot$OH), superoxide radicals ($\cdot O_2^-$), photo-generated holes (h$^+$), and photo-generated electrons (e$^-$), respectively. The catalytic activity was significantly inhibited when BQ or EDTA-2Na appeared in the reaction system. The results demonstrate that $\cdot O_2^-$ and h$^+$ are the main reactive species in the photocatalytic process of CuS@Cu-CDs.[52] AgNO$_3$ and TBA have a moderate

502 | *Environ. Sci.: Adv.*, 2023, **2**, 495–507

© 2023 The Author(s). Published by the Royal Society of Chemistry

Table 1 Comparison of CuS@Cu-CDs with other reported Fenton-like photocatalysts for the degradation of tetracycline

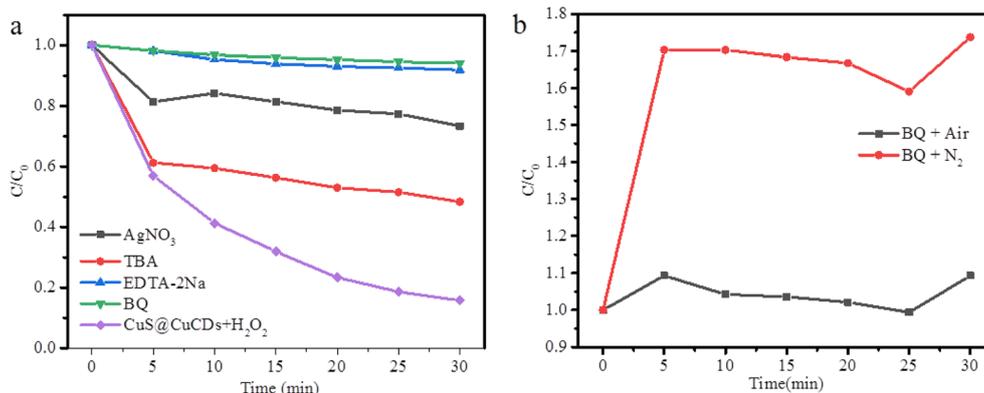| Catalyst	Dosage (g L^{-1})	H_2O_2 (mM)	TC (mg L^{-1})	pH	Time (min)	Degradation efficiency (%)	Ref.
yCeO$_2$/Fh	0.4	50.0	20	4.0	60	85.0	43
Mn$_2$O$_3$/pSiO$_2$	0.5	326.0	80	3.0–11.0	300	80.0	55
Fe/N–C	0.2	60.0	100	7.0	80	86.0	56
Fe$_3$O$_4$/α-FeOOH	0.75	20.0	20	5.0–9.0	80	100.0	57
CuS@Cu-CDs	0.5	7.0	100	5.6	30	85.0	This work

Fig. 8 (a) Active species trapping experiments and (b) $\cdot O_2^-$ quenching experiments under air and the solution treated with N_2 before the reaction on TC Fenton-like photodegradation by CuS@Cu-CDs [catalyst dosage] = 20 mg; [H_2O_2] = 7 mM; [TC] = 20 mg L^{-1}; pH = 5.6.

inhibitory influence on TC degradation, which indicated that e$^-$ and $\cdot OH$ played auxiliary roles in the photocatalytic degradation process.

To explore the contribution of the dissolved oxygen, we bubbled N_2 in the mixture of CuS@Cu-CDs, H_2O_2, and TC before the reaction. The result shows that the concentration of TC was much higher than that under air (Fig. 8b). It illuminated that the dissolved oxygen played an important key role in the reaction, which was indispensable for the formation of $\cdot O_2^-$.[53]

ESR analysis was also performed as supporting evidence for the above results. As shown in Fig. 9a, four peaks of $1:2:2:1$ proportion emerged in the DMPO–$\cdot OH$ spectra, and the intensity of signals increased in the presence of light, which stated that $\cdot OH$ was generated in the CuS@Cu-CDs Fenton-like system

and played key functions. The signal ratio of $1:1:1:1$ in DMPO–$\cdot O_2^-$ adducts was significantly enhanced by lighting (Fig. 9b). Combined with the fact of $\cdot O_2^-$ produced from O_2 absorbed on the photocatalyst surface via electron transformation,[43,53] we can deduce that $\cdot O_2^-$ played an important role in the oxidative degradation of TC. The combination of the above results reflected that the $\cdot O_2^-$ and $\cdot OH$ were the valid species during TC degradation in CuS@Cu-CDs Fenton-like system.

Possible degradation mechanism by CuS@Cu-CD composites

On the basis of the above experimental results, we propose the Fenton-like photocatalysis mechanism of CuS@Cu-CDs
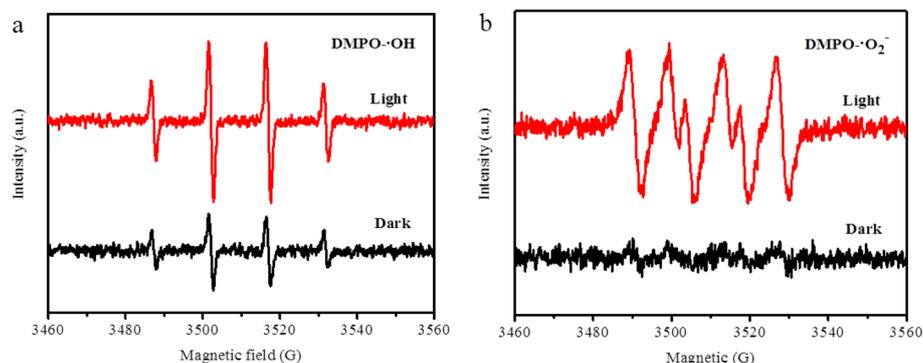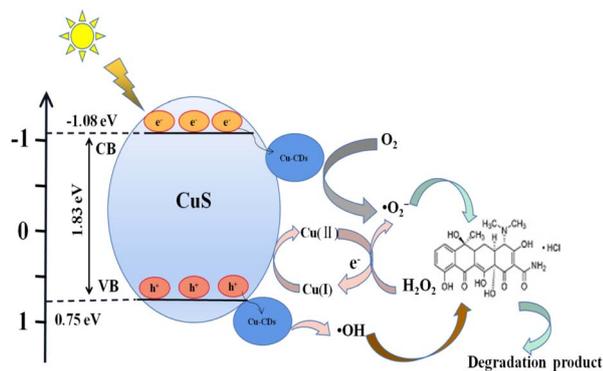

Fig. 9 ESR spectrum of CuS@Cu-CDs/H_2O_2 system (a) DMPO–$\cdot OH$ (b) DMPO–$\cdot O_2^-$.

© 2023 The Author(s). Published by the Royal Society of Chemistry

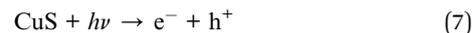*Environ. Sci.: Adv.*, 2023, **2**, 495–507 | **503**

Scheme 2 Proposed mechanism of photocatalytic degradation of TC.

(Scheme 2). First, TC in solutions can be adsorbed on the surface of CuS@Cu-CDs. The electron donor groups of TC were bound to the carboxylic groups of CDs *via* hydrogen bonds to form an electron-donor molecular structure intermediate.[54] Once illuminated under visible light, CuS absorbed energy and produced photogenerated e^- and h^+ on its conduction band, then photogenerated e^- transferred to the interface of CuS@Cu-CDs (eqn (7)), which prompted the reduction of Cu^{2+} to Cu^+ (eqn (8)). Cu^+ can react with O_2 to produce active radicals $\cdot O_2^-$ (eqn (9)) since the conduction band of CuS@Cu-CDs (-1.08 V) was more negative than $O_2/\cdot O_2^-$ potential (-0.046 V *vs.* NHE). Cu^{2+} was reduced by H_2O_2 to generate Cu^+ and simultaneously

produced $\cdot O_2^-$ (eqn (10)). Cu^+ could be oxidized by H_2O_2 to form Cu^{2+} and $\cdot OH$ (eqn (11)).[55] Undoubtedly, electrons play an important role in improving the efficiency of Fenton-like photocatalytic reactions by accelerating the Cu^{2+} to Cu^+ process, which promotes the regeneration of Cu^{2+} reaction centers. The holes (h^+) will be repelled to Cu-CDs, reacting with surface hydroxyl groups to form $OH\cdot$ radicals (eqn (12)).[52] $\cdot O_2^-$, h^+, and $\cdot OH$ on the composite surface diffused to the solution and broken TC down into small molecules, even mineralized into CO_2 and H_2O (eqn (13)).

$$CuS + h\nu \rightarrow e^- + h^+ \tag{7}$$

$$Cu^{2+} + e^- \rightarrow Cu^+ \tag{8}$$

$$Cu^+ + O_2 \rightarrow \cdot O_2^- + Cu^{2+} \tag{9}$$

$$Cu^{2+} + H_2O_2 \rightarrow Cu^+ + \cdot O_2^- + 2H^+ \text{ (major)} \tag{10}$$

$$Cu^+ + H_2O_2 \rightarrow Cu^{2+} + \cdot OH \text{ (minor)} \tag{11}$$

$$Cu\text{-}CDs\text{–}OH + h^+ \rightarrow Cu\text{-}CDs + \cdot OH \text{ (minor)} \tag{12}$$

$$\cdot O_2^-/h^+/\cdot OH + TC \rightarrow \text{degradation products} \tag{13}$$

As we know, Cu^{2+} was coordinated with $-COOH$ *via* bidentate coordination in Cu-CDs. The electron transfer between CDs and Cu^{2+} induced by π electron-withdrawing carboxylic groups
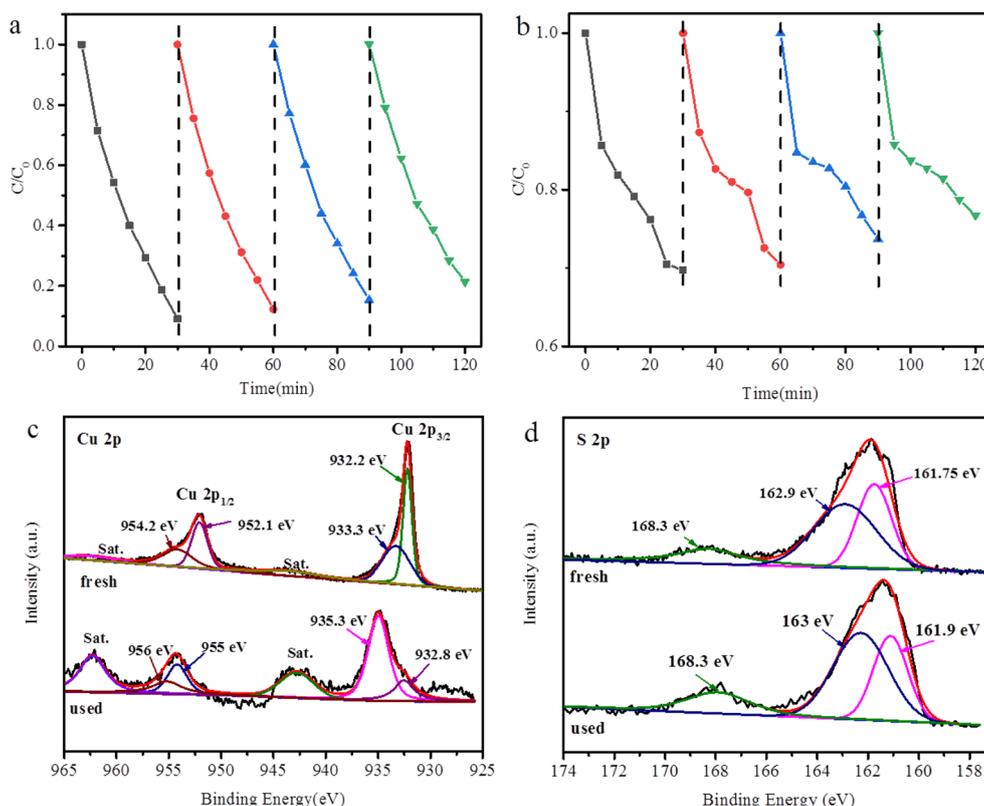

Fig. 10 Cycling runs with (a) CuS@Cu-CDs (b) CuS; XPS of CuS@Cu-CDs before and after the reaction (c) Cu 2p and (d) S 2p.

improved the electron migration of CuS.[54] Therefore, doping Cu^{2+} into CDs accelerated the electron transfer rate and prompted CuS generated electron (e^-) and hole (h^+) carriers. The synergistic effect between CuS and Cu-CDs endows the composites with high catalytic performance.

The stability of CuS@Cu-CDs was also investigated through the cyclic degradation of TC with the assistance of H_2O_2 under visible light irradiation. CuS@Cu-CDs and CuS (100 mg) were used in the recycling experiment. After the photocatalysis, the mixture was centrifuged and reduced by ascorbic acid to obtain a catalyst for the next reaction. The photocatalytic activity decreased by about 5–15% after four cycles (Fig. 10a). At this moment, Cu^{2+} concentration was almost undetectable. It demonstrated that hardly any copper ions leached during the cycle. However, the catalytic efficiency of CuS decreased by about 20–35% (Fig. 10b). The result indicated that the incorporation of Cu-CDs into CuS was therefore thought to enhance the visible light activity of CuS and also inhibit the photocorrosion of CuS, leading to a stable and durable photocatalytic activity.

To reveal the active centers of the catalyst, we carried out an XPS analysis of CuS@Cu-CDs after catalysis (Fig. 10c and d). The peaks of Cu 2p and S 2p in the used sample have visibly shifted to a high binding energy (1–3 eV). The fact suggested that there was interfacial interaction between CuS and Cu-CDs.[50] Compared with the freshly synthesized composites, the binding energies of Cu $2p_{3/2}$ and Cu $2p_{1/2}$ for the used catalyst shifted to higher positions (935.3.0 and 956.0 eV), indicating the increasing amount of Cu^{2+} after the Fenton-like reaction. Two satellite peaks of Cu $2p_{3/2}$ and Cu $2p_{1/2}$ were enhanced, further confirming the increased quantities of Cu^{2+} in the sample.[57] Furthermore, the comparison of Cu^+ peaks at 932.8, 955.0 eV and Cu^{2+} peaks at 935.3, 956.0 eV after the reaction shows a noticeable decrease in the peak intensity of Cu^+ relative to that of Cu^{2+}: the peak intensity ratio Cu^+/Cu^{2+} decreases from 1.98 : 1 to 0.69 : 1 upon the reaction. These results indicated that the interfacial electron cycle of Cu^+ and Cu^{2+} occurred on the surface of CuS@Cu-CDs and the oxidation of Cu^+ to Cu^{2+} by H_2O_2 after the reaction. The circulation played a key role in Fenton-like photocatalysis. The enhanced photocatalytic performance of CuS@Cu-CDs was derived from CDs doped with Cu^{2+}, which promoted electron migration and increased the separation of electrons and holes in CuS under irradiation.[10,58–60]

Conclusion

In summary, CuS@Cu-CDs exhibited excellent Fenton-like photocatalytic activity for the degradation of tetracycline. $\cdot O_2^-$ and h^+ radicals were the primary contributors, and $\cdot OH$ played an auxiliary role in the photodegradation process. The experiment indicated that the electron migration and the redistribution of local electrons in the catalyst system improved the Fenton-like activity. Our work may provide more thought in designing metal-doped carbon dot-decorated semiconductor composites that utilize visible light to solve environmental problems.

Conflicts of interest

The authors declare that they have no known competing financial interests or personal relationships that could have appeared to influence the work reported in this paper.

Acknowledgements

Notes and references

1 E. Neyens and J. Baeyens, A review of classic Fenton's peroxidation as an advanced oxidation technique, *J. Hazard. Mater.*, 2003, **98**, 33–50.

2 Y. P. Zhu, R. L. Zhu, Y. F. Xi, J. X. Zhu, G. Q. Zhu and H. P. He, Strategies for enhancing the heterogeneous Fenton catalytic reactivity: a review, *Appl. Catal. B: Environ.*, 2019, **255**, 117739.

3 A. D. Bokare and W. Choi, Review of iron-free Fenton-like systems for activating H_2O_2 in advanced oxidation processes, *J. Hazard. Mater.*, 2014, **275**, 121–135.

4 C. Dai, X. Tian, Y. Nie, H.-M. Lin, C. Yang, B. Han and Y. Wang, Surface facet of $CuFeO_2$ nanocatalyst: a key parameter for H_2O_2 activation in Fenton-like reaction and organic pollutant degradation, *Environ. Sci. Technol.*, 2018, **52**, 6518–6525.

5 H. Jin, X. Tian, Y. Nie, Z. Zhou, C. Yang, Y. Li and L. Lu, Oxygen vacancy promoted heterogeneous Fenton-like degradation of ofloxacin at pH 3.2-9.0 by Cu substituted magnetic Fe_3O_4@FeOOH nanocomposite, *Environ. Sci. Technol.*, 2017, **51**, 12699–12706.

6 T. Chen, Z. Zhu, H. Zhang, X. Shen, Y. Qiu and D. Yin, Enhanced removal of veterinary antibiotic florfenicol by a Cu-based Fenton-like catalyst with wide pH adaptability and high efficiency, *ACS Omega*, 2019, **4**, 1982–1994.

7 W. Cao, M. Han, L. Lyu, C. Hu and F. Xiao, Efficient Fenton-like process induced by fortified electron-rich O microcenter on the reduction state Cu-doped CNO polymer, *ACS Appl. Mater. Interfaces*, 2019, **11**, 16496–16505.

8 C. Zhang, L. Yan, X. Wang, X. Dong, R. Zhou, Z. Gu and Y. Zhao, Tumor microenvironment-responsive $Cu_2(OH)PO_4$ nanocrystals for selective and controllable radiosentization *via* the X-ray-triggered Fenton-like reaction, *Nano Lett.*, 2019, **19**, 1749–1757.

9 R. Rehman, S. K. Lahiri, A. Islam, P. Wei and Y. Xu, Self-assembled hierarchical Cu_xO@$C_{18}H_{36}O_2$ nanoflakes for superior Fenton-like catalysis over a wide range of pH, *ACS Omega*, 2021, **6**, 22188–22201.

10 H. H. Wang, L. L. Zhang, C. Hu, X. K. Wang, L. Lyu and G. D. Sheng, Enhanced degradation of organic pollutants over Cu-doped $LaAlO_3$ perovskite through heterogeneous Fenton-like reactions, *Chem. Eng. J.*, 2018, **332**, 572–581.

© 2023 The Author(s). Published by the Royal Society of Chemistry

Environ. Sci.: Adv., 2023, **2**, 495–507 | **505**

11 B. F. Sun, H. L. Li, X. Y. Li, X. W. Liu, C. H. Zhang, H. Y. Xu and X. S. Zhao, Degradation of organic dyes over Fenton-like Cu_2O-Cu/C catalysts, *Ind. Eng. Chem. Res.*, 2018, **57**, 14011–14021.

12 J. Q. Ma, N. Z. F. Jia, C. S. Shen, W. P. Liu and Y. Z. Wen, Stable cuprous active sites in Cu^+-graphitic carbon nitride: structure analysis and performance in Fenton-like reactions, *J. Hazard. Mater.*, 2019, **378**, 120782.

13 T. T. Cai, Q. Chang, B. Liu, C. H. Hao, J. L. Yang and S. L. Hu, Triggering photocatalytic activity of carbon dot based nanocomposites by a self-supplying peroxide, *J. Mater. Chem. A*, 2021, **9**, 8991–8997.

14 Z. Tang, P. Zhao, H. Wang, Y. Liu and W. Bu, Biomedicine meets Fenton chemistry, *Chem. Rev.*, 2021, **121**, 1981–2019.

15 K. J. Huang, J. Z. Zhang, Y. Liu and Y. M. Liu, Synthesis of reduced graphene oxide wrapped-copper sulfide hollow spheres as electrode material for supercapacitor, *Int. J. Hydrogen Energy*, 2015, **40**, 10158–10167.

16 Y. Wang, X. Liu, J. Liu, B. Han, X. Hu, F. Yang, Z. Xu, Y. Li, S. Jia, Z. Li and Y. Zhao, Carbon quantum dot implanted graphite carbon nitride nanotubes: excellent charge separation and enhanced photocatalytic hydrogen evolution, *Angew. Chem., Int. Ed.*, 2018, **57**, 5765–5771.

17 Y. Cheng, X. Wang, Y. Mei, D. Wang and C. Ji, ZnCDs/ZnO@ZIF-8 zeolite composites for the photocatalytic degradation of tetracycline, *Catalysts*, 2021, **11**, 934.

18 X. Wang, L. Li, Z. Fu and F. Cui, Carbon quantum dots decorated CuS nanocomposite for effective degradation of Methylene blue and antibacterial performance, *J. Mol. Liq.*, 2018, **268**, 578–586.

19 S. Xu, H. Zhu, W. Cao, Z. Wen, J. Wang, C. P. Francois-Xavier and T. Wintgens, Cu-Al_2O_3-g-C_3N_4 and Cu-Al_2O_3-C-dots with dual reaction centres for simultaneous enhancement of Fenton-like catalytic activity and selective H_2O_2 conversion to hydroxyl radicals, *Appl. Catal., B*, 2018, **234**, 223–233.

20 H. Peng, G. Ma, K. Sun, J. Mu, H. Wang and Z. Lei, High-performance supercapacitor based on multi-structural CuS@polypyrrole composites prepared by *in situ* oxidative polymerization, *J. Mater. Chem. A*, 2014, **2**, 3303–3307.

21 J. Hou, J. Yan, Q. Zhao, Y. Li, H. Ding and L. Ding, A novel one-pot route for large-scale preparation of highly photoluminescent carbon quantum dots powders, *Nanoscale*, 2013, **5**, 9558–9561.

22 L. Li, B. Yu and T. You, Nitrogen and sulfur Co-doped carbon dots for highly selective and sensitive detection of Hg (II) ions, *Biosens. Bioelectron.*, 2015, **74**, 263–269.

23 V. Gupta, N. Chaudhary, R. Srivastava, G. D. Sharma, R. Bhardwaj and S. Chand, Luminescent graphene quantum dots for organic photovoltaic devices, *J. Am. Chem. Soc.*, 2011, **133**, 9960–9963.

24 Z. Yang, M. Xu, Y. Liu, F. He, F. Gao, Y. Su, H. Wei and Y. Zhang, Nitrogen-doped, carbon-rich, highly photoluminescent carbon dots from ammonium citrate, *Nanoscale*, 2014, **6**, 1890–1895.

25 S. Zhu, Q. Meng, L. Wang, J. Zhang, Y. Song, H. Jin, K. Zhang, H. Sun, H. Wang and B. Yang, Highly photoluminescent carbon dots formulticolor patterning, sensors, and bioimaging, *Angew. Chem., Int. Ed.*, 2013, **125**, 3953–3957.

26 X. Chen, H. Li, Y. Wu, H. Wu, L. Wu, P. Tan, J. Pan and X. Xiong, Facile fabrication of novel porous graphitic carbon nitride/copper sulfide nanocomposites with enhanced visible light driven photocatalytic performance, *J. Colloid Interface Sci.*, 2016, **476**, 132–143.

27 X. Wen, L. Shi, G. Wen, Y. Li, C. Dong, J. Yang and S. Shuang, Green and facile synthesis of nitrogen-doped carbon nanodots for multicolor cellular imaging and Co^{2+}, sensing in living cells, *Sens. Actuators, B*, 2016, **235**, 179–187.

28 H. Wang, Z. Wei, H. Matsui and S. Zhou, Fe_3O_4/carbon quantum dots hybrid nanoflowers for highly active and recyclable visible-light driven photocatalyst, *J. Mater. Chem. A*, 2014, **2**, 15740–15745.

29 R. Liu, D. Wu, S. Liu, K. Koynov, W. Knoll and Q. Li, An aqueous route to multicolor photoluminescent carbon dots using silica spheres as carriers, *Angew. Chem., Int. Ed.*, 2009, **48**, 4598–4601.

30 Y. Y. Lu, Y. Y. Zhang, J. Zhang, Y. Shi, Z. Li, Z. C. Fengc and C. Li, In situ loading of CuS nanoflowers on rutile TiO_2 surface and their improved photocatalytic performance, *Appl. Surf. Sci.*, 2016, **370**, 312–319.

31 H. Wang, L. Zhang, C. Hu, X. Wang, L. Lyu and G. Sheng, Enhanced degradation of organic pollutants over Cu-doped $LaAlO_3$ perovskite through heterogeneous Fenton-like reactions, *Chem. Eng. J.*, 2018, **332**, 572–581.

32 F. E. Lopez-Suarez, S. Parres-Esclapez, A. Bueno-Lopez, M. J. Illan-Gomez, B. Ura and J. Trawczynski, Role of surface and lattice copper species in copper-containing (Mg/Sr)TiO_3 perovskite catalysts for soot combustion, *Appl. Catal., B*, 2009, **93**, 82–89.

33 P. Ajibade and N. Botha, Synthesis, optical and structural properties of copper sulfide nanocrystals from single molecule precursors, *Nanomaterials*, 2017, **7**, 32–44.

34 J. Xiao, X. Zhang and Y. Li, A Ternary g-C_3N_4/Pt/ZnO photoanode for efficient photoelectrochemical water splitting, *Int. J. Hydrogen Energy*, 2015, **40**, 9080–9087.

35 S. Zhao, M. Lan, X. Zhu, H. Xue, T. Ng, T. Meng, C. Lee, P. Wang and W. Zhang, Green synthesis of bifunctional fluorescent carbon dots from garlic for cellular imaging and free radical scavenging, *ACS Appl. Mater. Interfaces*, 2015, **7**, 17054–17060.

36 C. Mahala, M. D. Sharma and M. Basu, Type-II heterostructure of ZnO and carbon dots demonstrates enhanced photoanodic performance in photoelectrochemical water splitting, *Inorg. Chem.*, 2020, **59**, 6988–6999.

37 Y. Cheng, Y. Mei, S. Y. Deng and J. Li, In situ synthesis and photocatalytic performance of three dimensional composites CdS@DMSA-GO, *Chin. J. Inorg. Chem.*, 2020, **36**, 714–729.

38 Y. Li, Y. Jiang, Z. Ruan, K. Lin, Z. Yu, Z. Zheng, X. Xu and Y. Yuan, Simulation-guided synthesis of graphitic carbon nitride beads with 3D interconnected and continuous meso/macropore channels for enhanced light absorption

and photocatalytic performance, *J. Mater. Chem. A*, 2017, **5**, 21300–21312.

39 S. Bian, C. Zhou, P. Li, J. Liu, X. Dong and F. Xi, Graphene quantum dots decorated titania nanosheets heterojunction efficient charge separation and enhanced visible-light photocatalytic performance, *ChemCatChem*, 2017, **9**, 3349–3357.

40 M. Bilal, S. Mehmood, T. Rasheed and H. M. N. Iqbal, Antibiotics traces in the aquatic environment: persistence and adverse environmental impact, *Curr. Opin. Environ. Sci. Health*, 2020, **13**, 68–74.

41 D. Cheng, H. H. Ngo, W. Guo, S. W. Chang, D. D. Nguyen, Y. Liu, Q. Wei and D. Wei, A critical review on antibiotics and hormones in swine wastewater: water pollution problems and control approaches, *J. Hazard. Mater.*, 2020, **387**, 121682.

42 P. Välitalo, A. Kruglova, A. Mikola and R. Vahala, Toxicological impacts of antibiotics on aquatic micro-organisms: a mini-review, *Int. J. Hyg. Environ. Health*, 2017, **220**, 558–569.

43 X. Huang, N. Zhu, F. Mao, Y. Ding, S. Zhang, H. Liu, F. Li, P. Wu, Z. Dang and Y. Ke, Enhanced heterogeneous photo-Fenton catalytic degradation of tetracycline over yCeO$_2$/Fh composites: performance, degradation pathways, Fe^{2+} regeneration and mechanism, *Chem. Eng. J.*, 2020, **392**, 123636.

44 A. Babuponnusami and K. Muthukumar, Advanced oxidation of phenol: a comparison between Fenton, electro-Fenton, sono-electro-Fenton and photo-electro-Fenton processes, *Chem. Eng. J.*, 2012, **183**, 1–9.

45 J. L. Wang and L. J. Xu, Advanced oxidation processes for wastewater treatment: formation of hydroxyl radical and application, *Crit. Rev. Environ. Sci. Technol.*, 2012, **42**, 251–325.

46 C. Lai, F. L. Huang, G. M. Zeng, D. L. Huang, L. Qin, M. Cheng, C. Zhang, B. Li, H. Yi, S. Liu, L. Li and L. Chen, Fabrication of novel magnetic MnFe$_2$O$_4$/bio-char composite and heterogeneous photo-Fenton degradation of tetracycline in near neutral pH, *Chemosphere*, 2019, **224**, 910–921.

47 H. Zheng, J. Bao, Y. Huang, L. Xiang, B. Faheem, J. Ren, M. N. Du and D. D. D. Nadagouda, Efficient degradation of atrazine with porous sulfurized Fe$_2$O$_3$ as catalyst for peroxymonosulfate activation, *Appl. Catal., B*, 2019, **259**, 118056.

48 H. Liang, R. Liu, X. An, C. Hu, X. Zhang and H. Liu, Bimetal-organic frameworks with coordinatively unsaturated metal sites for highly efficient Fenton-like catalysis, *Chem. Eng. J.*, 2021, **414**, 128669.

49 Q. Zhang, M. Yu, N. Wang, J. Qian, Y. Gu, F. Du, Y. Lin, F. Chen, Z. Chen, Z. Wu and L.-B. Sun, Porous Mn$_2$O$_3$/

pSiO$_2$ nanocomposites on bio-scaffolds for tetracycline degradation, *ACS Appl. Nano Mater.*, 2022, **5**, 9117–9128.

50 Y. Yang, X. Zhang, Q. Chen, S. Li, H. Chai and Y. Huang, Ultrasound-assisted removal of tetracycline by a Fe/N−C hybrids/H$_2$O$_2$ Fenton-like system, *ACS Omega*, 2018, **3**, 15870–15878.

51 X. Huang, H. Zhou, X. Yue, S. Ran and J. Zhu, Novel magnetic Fe$_3$O$_4$/α-FeOOH nanocomposites and their enhanced mechanism for tetracycline hydrochloride removal in the visible photo-Fenton process, *ACS Omega*, 2021, **6**, 9095–9103.

52 N. Li, W. Fu, C. Chen, M. Liu, F. Xue, Q. Shen and J. Zhou, Controlling the core–shell structure of CuS@CdS heterojunction *via* seeded growth with tunable photocatalytic activity, *ACS Sustainable Chem. Eng.*, 2018, **6**, 15867–15875.

53 H. Wang, L. Zhang, C. Hu and X. Wang, Enhanced Fenton-like catalytic performance of Cu-Al/KIT-6 and the key role of O$_2$ in triggering reaction, *Chem. Eng. J.*, 2020, **387**, 124006.

54 T. Zhang, Y. Wen, Z. Pan, Y. Kuwahara, K. Mori, H. Yamashita, Y. Zhao and X. Qian, Overcoming acidic H$_2$O$_2$/Fe(II/III) redox-induced low H$_2$O$_2$ utilization efficiency by carbon quantum dots Fenton-like catalysis, *Environ. Sci. Technol.*, 2022, **56**, 2617–2625.

55 W. Xiang, T. Zhou, Y. Wang, M. Huang, X. Wu, J. Mao, X. Lu and B. Zhang, Catalytic oxidation of diclofenac by hydroxylamine enhanced Cu nanoparticles and the efficient neutral heterogeneous homogeneous reactive copper cycle, *Water Res.*, 2019, **153**, 274–283.

56 D. Xiang, X. Hao and Z. Jin, Cu/CdS/MnO$_x$ nanostructure-based photocatalyst for photocatalytic hydrogen evolution, *ACS Appl. Nano Mater.*, 2021, **4**, 13848–13860.

57 F. C. De Godoi, E. Rodriguez-Castellon, E. Guibal and M. M. Beppu, An XPS study of chromate and vanadate sorption mechanism by chitosan membrane containing copper nanoparticles, *Chem. Eng. J.*, 2013, **234**, 423.

58 G. K. Grandhi, K. Swathi, K. S. Narayan and R. Viswanatha, Cu doping in ligand free CdS nanocrystals: conductivity and electronic structure study, *J. Phys. Chem. Lett.*, 2014, **5**, 2382–2389.

59 Q. Xu, Y. Liu, R. Su, L. Cai, B. Li, Y. Zhang, L. Zhang, Y. Wang, Y. Wang, N. Li, X. Gong, Z. Gu, Y. Chen, Y. Tan, C. Dong and T. S. Sreeprasad, Highly fluorescent Zn-doped carbon dots as Fenton reaction-based bio-sensors: an integrative experimental-theoretical consideration, *Nanoscale*, 2016, **8**, 17919–17927.

60 W. Wu, L. Zhan, W. Fan, J. Song, X. Li, Z. Li, R. Wang, J. Zhang, J. Zheng, M. Wu and H. Zeng, Cu–N dopants boost electron transfer and photooxidation reactions of carbon dots, *Angew. Chem., Int. Ed.*, 2015, **54**, 6540–6544.

© 2023 The Author(s). Published by the Royal Society of Chemistry

Environ. Sci.: Adv., 2023, **2**, 495–507 | **507**